*Journal of Applied Electrochemistry* **33**: 1169–1173, 2003.



# Electrochemical properties of layered $Li[Ni_{1/2}Mn_{1/2}]O_2$ cathode material synthesised by ultrasonic spray pyrolysis

S.H. PARK[1], Y.S. LEE[2], Y. SATO[3] and Y.-K. SUN[1,*]
[1]*Department of Chemical Engineering, Hanyang University, Seoul 133-791, South Korea*
[2]*High-Tech Research Center, Kanagawa University, Yokohama 221-8686, Japan*
[3]*Department of Applied Chemistry, Kanagawa University, Yokohama 221-8686, Japan*
*(*author for correspondence, e-mail: yksun@hanyang.ac.kr)*

Received 31 March 2003; accepted in revised form 9 July 2003

*Key words:* cathode, layered, $LiNi_{1/2}Mn_{1/2}O_2$, lithium, manganese

**Abstract**

Layered $Li[Ni_{1/2}Mn_{1/2}]O_2$ was synthesized by an ultrasonic spray pyrolysis method. The $Li[Ni_{1/2}Mn_{1/2}]O_2$ powder was characterized by means of X-ray diffraction, charge/discharge test, and cyclic voltammetry. The discharge capacity increases linearly with increase of the upper cut-off voltage limit and attains a high discharge capacity of 187 mA h $g^{-1}$ between 2.8 and 4.6 V with excellent cyclability. A cyclic voltammetric study of the $Li[Ni_{1/2}Mn_{1/2}]O_2$ electrode showed only one redox peak implying no structural phase change during cycling.

## 1. Introduction

Layered lithium transition metal oxides, $LiMO_2$ (M = Co, Ni, Mn) with a hexagonal $\alpha$-$NaFeO_2$ structure, have been expanded in the last a few years in the application of rechargeable batteries as cathode materials for lithium secondary batteries. $LiCoO_2$ has been commercialized but still has limits due to its high cost and toxicity. Layered $LiNiO_2$ and $LiMnO_2$ have been extensively studied as possible alternatives to $LiCoO_2$. Although there has been much progress in optimizing the two materials, there are still problems for practical applications. $LiNiO_2$ cannot be used in its current form because it is known to be difficult to synthesize in the stoichiometric form and delithiated $Li_{1-x}NiO_2$ decompose exothermally at around 200 °C [1–3]. Also, the $LiMnO_2$ form is not as thermodynamically stable as the layered structure, especially the orthorhombic phase of $LiMnO_2$ [4]. The $Mn^{3+}$ ($d^4$) ions cause a cooperative distortion of the $MnO_6$ octahedra due to Jahn–Teller stabilization, leading to a monoclinic unit cell. When Li was deintercalated from $LiMnO_2$, both the *m*- and *o*-$LiMnO_2$ underwent a detrimental phase transformation to a spinel-like phase through minor atomic rearrangements, leading to the eventual deterioration of electrode performance [5, 6].

Recently, Ohzuku and Makimura reported a new concept of one-to-one solid solution with atomic scale of $LiNiO_2$ and $LiMnO_2$, i.e., $Li[Ni_{1/2}Mn_{1/2}]O_2$ [7]. The $Li[Ni_{1/2}Mn_{1/2}]O_2$ delivered a reversible capacity of 150 mA h $g^{-1}$ in the voltage range 3.0–4.3 V with no indication of transformation to the spinel phase during electrochemical cycling. Yoon et al. reported that the $Ni^{2+}$ and $Mn^{4+}$ coexist in the layered $Li[Ni_{1/2}Mn_{1/2}]O_2$ structure and the $Ni^{2+}$ ion is oxidized to $Ni^{4+}$, while $Mn^{4+}$ ions remain mostly unchanged as Li is deintercalated from the host material [8]. The stable cycling behavior of the $Li[Ni_{1/2}Mn_{1/2}]O_2$ material may be attributed to the stable tetravalent oxidation state of Mn ions during electrochemical cycling.

Considerable improvements of cathode materials with good battery performance have been made by the use of solution methods such as the sol–gel method, the coprecipitation method and the spray pyrolysis method [7–12]. Among the solution methods, spray pyrolysis is an effective technique leading to good stoichiometric control, homogeneous particle size and short production time. It is also a one-step method. Recently, Taniguchi et al. reported that spherical spinel $LiMn_2O_4$ powders could be synthesized using spray pyrolysis by varying the gas flow rate and temperature profiles in the reactor [12].

In this study, we report on the synthesis and electrochemical characteristics of $Li[Ni_{1/2}Mn_{1/2}]O_2$ powders synthesized by an ultrasonic spray pyrolysis method.

## 2. Experimental

$Li[Ni_{1/2}Mn_{1/2}]O_2$ powder was prepared as follows: $[Ni_{1/2}Mn_{1/2}]O_y$ precursor was first synthesized using a spray pyrolysis method. Nickel nitrate hexahydrate ($Ni(NO_3)_2 \cdot 6H_2O$, Aldrich, USA) and manganese nitrate hydrate ($Mn(NO_3)_2 \cdot 4H_2O$, Sigma, USA) salts

were used as starting materials for the synthesis of $[Ni_{1/2}Mn_{1/2}]O_y$ powder. At first, a stoichiometric amount of Ni and Mn nitrate salts (cationic ratio of Ni:Mn = 1:1) was dissolved in distilled water. The dissolved solution was added to a continuously agitated aqueous citric acid solution. Citric acid ($C_6H_8O_7 \cdot H_2O$, Aldrich, USA) was used as a polymeric agent for the reaction. The molar concentration of citric acid was fixed at 0.2 M. The starting solution was atomized using an ultrasonic nebulizer with a resonant frequency of 1.7 MHz. The aerosol stream was introduced into the vertical quartz reactor heated at 500 °C. The inner diameter and length of the quartz reactor were 50 and 1200 mm, respectively. The flow rate of air used as a carrier gas was 10 L $min^{-1}$. The prepared powder was thoroughly mixed with $LiOH \cdot H_2O$. After the mixture was sufficiently ground, these were heated again at 900 °C in a box furnace with a heating rate of 1 °C $min^{-1}$.

The thermal decomposition behavior of the precursors was examined by thermogravimetric analysis and differential thermal analysis using a TG-8110 thermal analyzer system (TGA, DTA, TAS 100, Rigaku, Japan). The heating/cooling rate was 5 °C $min^{-1}$. A powder X-ray diffraction (XRD, Rint-2000, Rigaku, Japan) measurement using $CuK_\alpha$ radiation was employed to identify the crystalline phase of the synthesized material. Rietveld refinement was then performed on the XRD profiles to obtain lattice constants. Particle morphology of the powders after calcination was observed using a scanning electron microscope (SEM, JSM 6400, JEOL, Japan). The average particle size and the particle size distribution were determined by a particle size analyzer (UPA 150, Mictrotrac Co. USA).

A three-electrode glass cell was used for cyclic voltammetry (CV). The working electrode consisted of 3 mg of the active material and 2.2 mg of conducting binder (Teflonized acetylene black, TAB), which was pressed onto stainless steel mesh. The counter and reference electrodes were prepared by pressing lithium foil onto stainless steel gauze. The CV measurement was performed with an Arbin Instruments Model MSTAT4 battery test system at 100 $\mu V\ s^{-1}$ scan rate between the voltage limits of 2.5–4.0 V. All assembling of the cell was carried out in a dry box filled with argon gas. Galvanostatic charge/discharge cycling was performed in a 2032-type coin cell. For the fabrication of the positive electrode, 20 mg of $Li[Ni_{1/2}Mn_{1/2}]O_2$ compound was mixed with 12 mg of conductive binder (8 mg of TAB and 4 mg of graphite). The mixture was pressed on 200 $mm^2$ stainless steel mesh used as the current collector and dried at 130 °C for 10 h in a vacuum oven. The test cell was made of a cathode and a lithium metal anode (Cyprus Foote Mineral Co.) separated by a porous polypropylene film (Celgard 3401). The electrolyte solution was 1 M $LiPF_6$ in a mixture of ethylene carbonate (EC) and diethyl carbonate (DEC) in a 1:1 volume ratio. The cell was assembled in an argon-filled glove box. The charge/discharge measurements were carried out between 2.8 and 4.3, 4.4, 4.5, and 4.6 V potential ranges at a current density of 0.2 mA $cm^{-2}$ (20 mA $g^{-1}$).

## 3. Results and discussion

Figure 1 shows the thermogravimetric analysis of $Ni(NO_3) \cdot 6H_2O$, $Mn(NO_3)_2 \cdot 4H_2O$, and $C_6H_8O_7 \cdot H_2O$ mixture. The first weight loss in the temperature range below 200 °C is due to the removal of water from each chemical. The second weight loss in the temperature region of below 400 °C is related to the decomposition of nitrate ions and organic moieties. The weight loss of the starting materials is almost terminated at 500 °C, indicating that the organic compounds can removed completely at temperatures lower than 500 °C. From the thermal analysis, we determined that the precursor of $[Ni_{1/2}Mn_{1/2}]O_y$ can be obtained from a temperature around 500 °C.

The XRD pattern of the $[Ni_{1/2}Mn_{1/2}]O_y$ precursor obtained at 500 °C is shown in Figure 2(a). Although the XRD pattern has a very lower crystallinity, it was found that the precursor is composed of a mixture of $Mn_3O_4$ and NiO. Figure 2(b) shows the XRD pattern of the $Li[Ni_{1/2}Mn_{1/2}]O_2$ powder calcined at 900 °C in air. All peaks can be indexed based on a hexagonal $\alpha$-$NaFeO_2$ structure with a space group of $R\bar{3}m$. The XRD pattern of the $Li[Ni_{1/2}Mn_{1/2}]O_2$ material shows a phase-pure layered structure showing good crystallinity(FWHM of 003 peak is 0.2 Θ). This may be ascribed to the homogeneous powder precursor, in which cations such as Ni and Mn are uniformly distributed at an atomic scale. This XRD pattern also shows a large integrated peak ratio (003) to (104) and a clear split of the (108) and (110) peaks, which indicates the lower disorder in the host structure [13]. The lattice constants of $Li[Ni_{1/2}Mn_{1/2}]O_2$ are $a = 2.880$ Å and $c = 14.276$ Å, as calculated by Rietveld refinement from the XRD data.

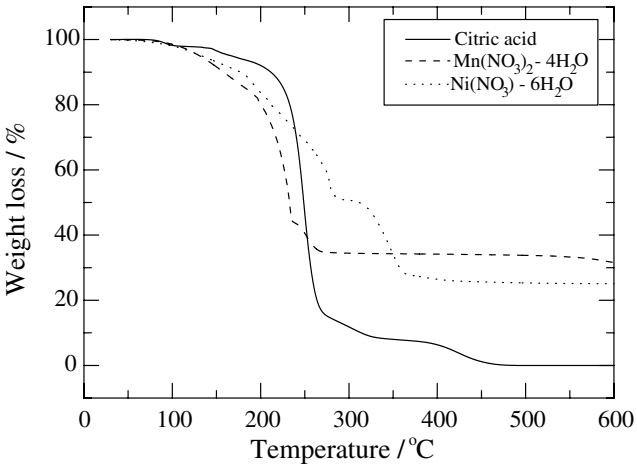


*Fig. 1.* Thermogravimetric analysis of the starting materials. The mixture was dried in a vacuum oven at 25 °C prior to the thermal analysis and the heating rate was 5 °C $min^{-1}$ in air.

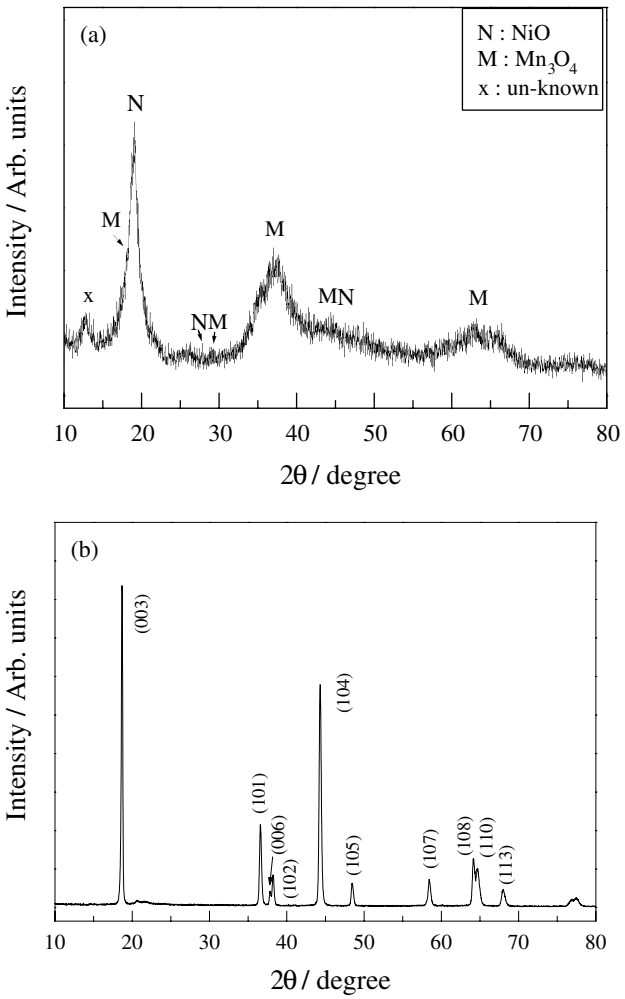


*Fig. 2.* Powder XRD patterns of (a) $[Ni_{1/2}Mn_{1/2}]O_y$ prepared at 500 °C, and (b) $Li[Ni_{1/2}Mn_{1/2}]O_2$ calcined at 900 °C.

Figure 3 shows SEM for the $[Ni_{1/2}Mn_{1/2}]O_y$ and $Li[Ni_{1/2}Mn_{1/2}]O_2$ powders. Figure 3(a) shows that the as-prepared powder has a spherical morphology with particles of about 2–3 $\mu$m. The particles of $[Ni_{1/2}Mn_{1/2}]O_y$ maintain their round shape. On the other hand, $Li[Ni_{1/2}Mn_{1/2}]O_2$ powder shows spherical type agglomerates with particle size of about 2 $\mu$m, composed of lots of spherical primary particles of approximately 200 nm diameter. However, the $Li[Ni_{1/2}Mn_{1/2}]O_2$ particles changed into a walnut like shape. It may be assumed that the $[Ni_{1/2}Mn_{1/2}]O_y$ particles are completely changed by combining with the lithium source during calcinations process. This is a typical problem associated with the formation of hollow oxide particles by spray pyrolysis using nitrates as starting material [14, 15]. The particle size distribution obtained for the $[Ni_{1/2}Mn_{1/2}]O_y$ and $Li[Ni_{1/2}Mn_{1/2}]O_2$ powders is shown in Figure 4. The particles of $Li[Ni_{1/2}Mn_{1/2}]O_2$ are smaller than those of $[Ni_{1/2}Mn_{1/2}]O_y$ as confirmed in Figure 3. Furthermore, most particles of $Li[Ni_{1/2}Mn_{1/2}]O_2$ are within a narrow size distribution and have smaller average particle size distribution compared to those of $[Ni_{1/2}Mn_{1/2}]O_y$. This may result from the shrinkage of $[Ni_{1/2}Mn_{1/2}]O_y$ powder during high temperature calcination at 900 °C.

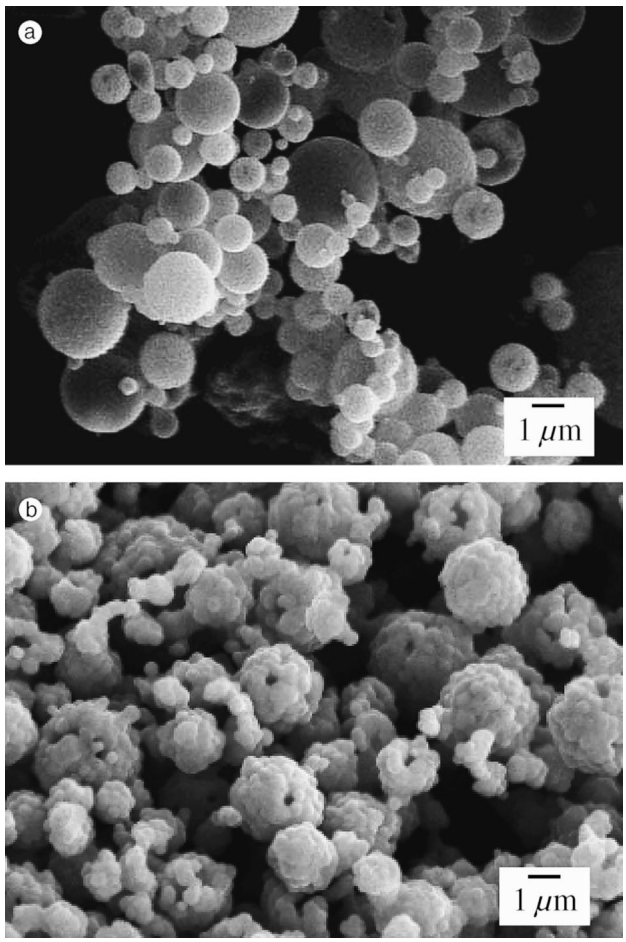


*Fig. 3.* SEM for (a) $[Ni_{1/2}Mn_{1/2}]O_y$ prepared at 500 °C, and (b) $Li[Ni_{1/2}Mn_{1/2}]O_2$ calcined at 900 °C.

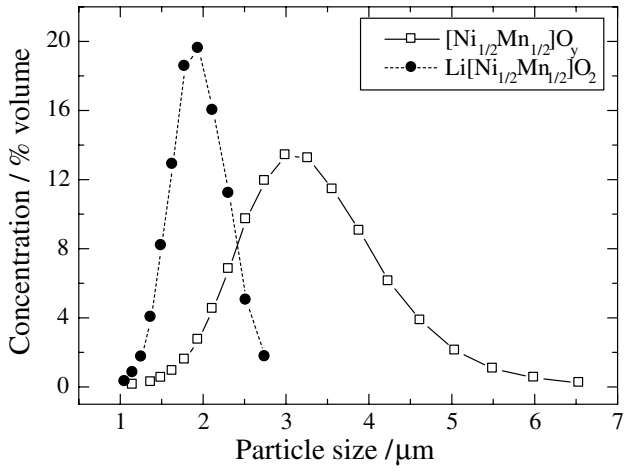


*Fig. 4.* Particle size distributions of $[Ni_{1/2}Mn_{1/2}]O_y$ and $Li[Ni_{1/2}Mn_{1/2}]$ $O_2$ powders.

Figure 5 shows the charge/discharge curves and specific discharge capacities for the $Li/Li[Ni_{1/2}Mn_{1/2}]$ $O_2$ cells as a function of cycle number between 2.8–4.3, 2.8–4.4, 2.8–4.5, and 2.8–4.6 V at a constant current density of 0.2 mA $cm^{-2}$ (20 mA $g^{-1}$). All $Li/Li[Ni_{1/2}Mn_{1/2}]O_2$ cells showed smooth and monotonic voltage profiles as reported by other groups [7, 9]. The $Li/Li[Ni_{1/2}$-

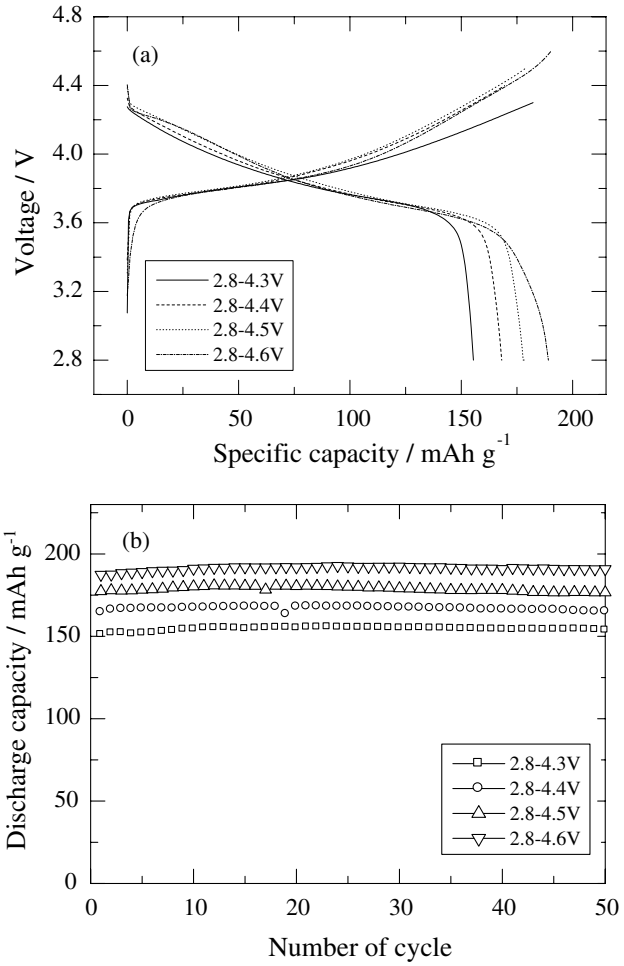


*Fig. 5.* (a) Charge/discharge curves, and (b) specific discharge capacity of Li/ $Li[Ni_{1/2}Mn_{1/2}]O_2$ cells with various cut-off voltages as a function of cycle number at 30 °C.

$Mn_{1/2}]O_2$ cell between 2.8 and 4.4 V exhibits a small irreversible capacity ($C_{dis}/C_{cha}$) of 14% in the first cycle, which is lower than that of lithium rich layered oxide material, $Li[Li_{(1-2x)/3}Ni_xMn_{(2-x)/3}]O_2$ [10, 16]. Although not shown here, the voltage profiles for a $Li/Li[Ni_{1/2}$-$Mn_{1/2}]O_2$ cell were not changed even after 50 cycles, which indicates that structural degradation did not occur by repeatative lithium insertion/extraction into the host structure during cycling. Yoon et al. reported that Ni and Mn ions are in the $2^+$ and $4^+$ oxidation state respectively, as confirmed by Mn and Ni K-edge XANES and electrochemical processes involve between $Ni^{2+}$ and $Ni^{4+}$ with two electron transfer [8]. The discharge capacities of the $Li/Li[Ni_{1/2}Mn_{1/2}]O_2$ cell increase linearly by increasing the upper cut-off voltage limit. In the voltage range 2.8–4.3 V, −4.4 V, −4.5 V, and −4.6 V, the discharge capacities of the $Li[Ni_{1/2}Mn_{1/2}]$-$O_2$ electrode were 155, 166, 177, and 187 mA h g$^{-1}$, respectively. All the cells showed excellent cycle retention without capacity loss up to 50 cycles.

Figure 6 shows the charge/discharge curves of Li/ $Li[Ni_{1/2}Mn_{1/2}]O_2$ cells at various current densities (C-rate) within voltage limits of 2.8–4.4 V. Each cell was charged using a current density of 0.32 mA cm$^{-2}$ (0.2 C rate) and discharged at various currents. The discharge capacities of each cell slowly decreased with increasing current density. The discharge capacity at a current density of 1.6 (1 C) and 6.4 mA cm$^{-2}$ (4 C) reached 92 and 75%, compared to that of 0.16 mA cm$^{-2}$ (0.1 C), respectively. We believe that this is one of the best results for a $Li/Li[Ni_{1/2}Mn_{1/2}]O_2$ cell in a high current density test (4 C) and $Li[Ni_{1/2}Mn_{1/2}]O_2$ is a good candidate cathode material for large-scale lithium secondary batteries.

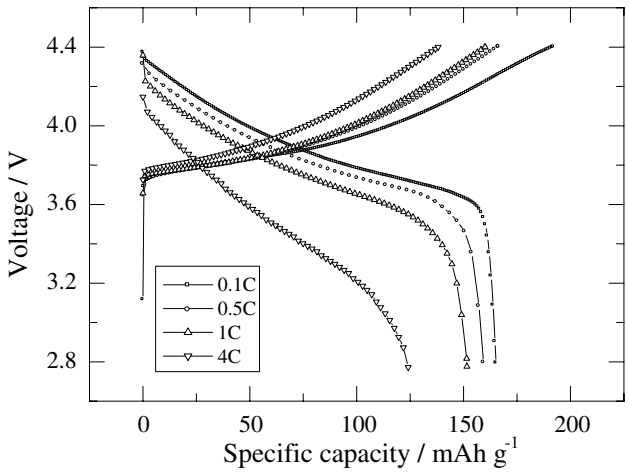


*Fig. 6.* Charge/discharge curves of $Li/Li[Ni_{1/2}Mn_{1/2}]O_2$ cells at various current densities between 2.8 and 4.4 V. Each cell was charged using a current density of 0.32 mA cm$^{-2}$ (0.2 C rate) and discharged using various current densities.

Figure 7 shows the cyclic voltammogram of $Li[Ni_{1/2}$-$Mn_{1/2}]O_2$ for the first 5 cycles between 2.5 and 4.6 V. Similar to the charge/discharge curve shown in Figure 6(a), the profile of the first anodic peak was slightly different from the subsequent ones. The first anodic scan has two oxidation peaks; a major peak centered at 4.02 V and a minor one at 4.5 V, corresponding to the irreversible capacity observed in the first charge profile (Figure 6(a)). The peak at 4.02 V in the first anodic scan

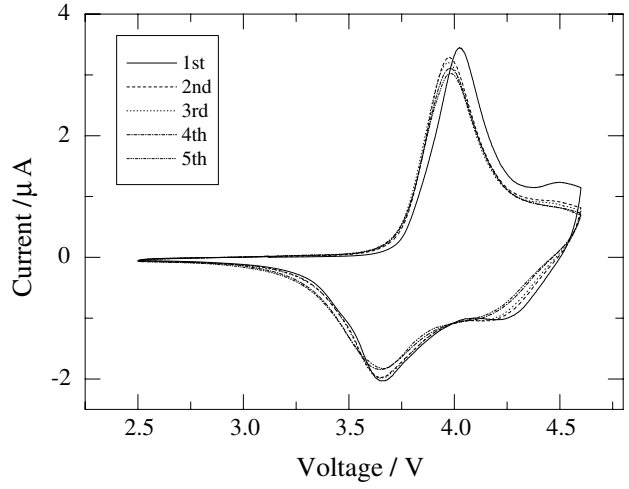


*Fig. 7.* Cyclic voltammogram of $Li[Ni_{1/2}Mn_{1/2}]O_2$ between 2.5 and 4.6 V at a scan rate of 100 $\mu$V s$^{-1}$.

is shifted by 0.05 V to the lower voltage region and remains unchanged from the subsequent cycles. The reduction peak observed at 4.3 V during the first cycle disappears after 3 cycles and there is a single major peak centered at 3.97 V in the cathodic process. This phenomenon is related to the initial activation process and/or stabilization of the $Li[Ni_{1/2}Mn_{1/2}]O_2$ electrode and implies that structural degradation is not expected during the lithium extraction/insertion process of the $Li[Ni_{1/2}Mn_{1/2}]O_2$ electrode unlike $LiNiO_2$ [1, 16].

## 4. Conclusion

Layered $Li[Ni_{1/2}Mn_{1/2}]O_2$ powders with high homogeneity, spherical morphology and high capacity have been synthesized by the ultrasonic spray pyrolysis method. The $Li[Ni_{1/2}Mn_{1/2}]O_2$ electrode delivered a high initial discharge capacity of 187 mA h $g^{-1}$ between 2.8 and 4.6 V at a current density of 0.2 mA $cm^{-2}$ (20 mA $g^{-1}$) with excellent cyclability. Charge/discharge and cyclic voltammogram studies of the $Li[Ni_{1/2}Mn_{1/2}]O_2$ electrode showed only one redox peak, indicating that structural phase transitions did not occur during electrochemical cycling.

## Acknowledgements

This research was performed with the financial support of 'Center for Nanostructured Materials Technology' under '21st Century Frontier R&D Programs' of the Ministry of Science and Technology, and was partly supported by the Korea Science and Engineering Foundation via Research Center for Energy Conversion and Storage, Korea.

## References

1. J.R. Dahn, E.W. Fuller, M. Obrovac and U. von Sacken, *Solid State Ionics* **69** (1994) 265.
2. H. Arai and Y. Sakurai, *J. Power Sources* **81–82** (1999) 401.
3. T. Ohzuku, A. Ueda and M. Kouguchi, *J. Electrochem. Soc.* **142** (1995) 4033.
4. B. Ammundsen and J. Paulsen, *Adv. Mat.* **13** (2001) 943.
5. G. Vitins and K. West, *J. Electrochem. Soc.* **144** (1997) 2587.
6. Y.-I. Jang, B. Huang, Y.-M. Chiang and D.R. Sadoway, *Electrochem. & Solid-State Lett.* **1** (1998) 13.
7. T. Ohzuku and Y. Makimura, *Chem. Lett.* (2001) 744.
8. W.-S. Yoon, Y. Paik, X.-Q. Yang, M. Balasubramanian, J. McBreen and C.P. Grey, *Electrochem. & Solid-State Lett.* **5** (2002) A263.
9. Z. Lu, D.D. MacNeil and J.R. Dahn, *Electrochem. & Solid-State Lett.* **4** (2001) A200.
10. S.-S. Shin, Y.-K. Sun and K. Amine, *J. Power Sources* **112** (2002) 634.
11. T. Ogihara, N. Ogata, K. Katayama, Y. Azuma and N. Mizutani, *Electrochemistry* **68** (2000) 162.
12. I. Taniguchi, C.K. Lim, D. Song and M. Wakihara, *Solid Stat Ionics* **146** (2002) 239.
13. T. Ohzuku, A. Ueda and M. Kouguchi, *J. Electrochem. Soc.* **142** (1995) 4033.
14. S. Jain, D.J. Skamser and T.T. Kodas, *Aerosol Sci. Tech.* **27** (1997) 575.
15. S. Che, K. Takada, O. Sakurai, K. Shinozaki and N. Mizutani, *J. Mater, Sci.* **34** (1999) 1313.
16. J.-H. Kim, C.S. Yoon and Y.-K. Sun, *J. Electrochem. Soc.* **150** (2003) A538.